The Role of Morphological Computation of the Goat Hoof in Slip Reduction

Sara-Adela Abad[1], Nantachai Sornkarn[1] and Thrishantha Nanayakkara[1]

***Abstract*— The remarkable ability of goats to maintain stability during climbing cliffs or trees provides a valuable opportunity to understand some of the secrets of stable legged locomotion on unstructured terrains. This paper, for the first time, presents analytical and experimental explanations as to how the morphological computation at the goat hoof makes a significant contribution to slip reduction on both smooth and rough surfaces. We conducted experiments using a laboratory made hoof and compared its dynamic behavior against a rounded foot. We recorded forces and position of the hoof to analyze the effect of its shape and the individual contributions from 3-joints in the hoof on the work required to slip. Results state that the work required to move the hoof is more than 3 times that required to move a rounded foot. Additionally, the variables in the transient state are affected not only by the number and type of joints but also by the interaction with the environment. These findings promote the development of new types of feet for robots for all terrain conditions with greater stability and less control complexity.**

I. Introduction

Legged locomotion offers many advantages such as the opportunity to come into contact with a rough terrain at selected locations, ability to control the direction of contact forces, and deform soft soil to aid forward movement. However, the punctuated forces at each foot-ground collision produce uncertainty of slip, and the piece-wise non-linear interaction dynamics experienced during each collision [1] makes walking harder than many other modes of locomotion.

Technology on robotic legged walkers has made significant advances in the recent past starting from simple passive dynamic walking experiments [2] in 1980's to the Big Dog [3] and the LittleDog [4] developed by Boston Dynamics. Though they have demonstrated exceptional capabilities in outdoor locomotion, they use basic rounded feet. We predict that a better foot design will help to improve their stability and energy efficiency on unstructured and slippery terrains.

Some other attempts to develop legged walkers include Dagsi Whegs^{TM}[5], RHex [6], MSROX [7], and IMPASS [8]. RHex in particular follows the biological inspiration from cockroaches that there is no defined border separating the foot and the rest of the leg. However, the dynamic analysis of RHex legs in the form of an elastic template shows the importance of the role of morphological computation in the dynamic performance of the walker. Throughout this paper, the notion - *morphological computation* - refers to the computations done by bodily circuits in contact with the environment.

Most walkers use simple foot designs that do not demonstrate morphological computational capabilities of their biological counterparts like the hoofs of animals known for having an ecological niche in muddy and hilly terrains. For instance, IMPASS is stable due to its whegs that are rimless wheels with individually actuated spokes; but its control can be more complex than that of RHex. This increases the power consumption for uneven terrain. This is clearly illustrated in Dagsi Whegs^{TM}[5]. It requires the same power for walking over three hours on relatively level terrain as for climbing for 45 minutes. Therefore, power consumption, control complexity, and stability remain as the main limitations.

In this paper we introduce a novel multibody compliant robotic foot inspired by the hoof of goats for terrains with high variability. It has the following advantages: *a)* it has interdigital ligaments that allow spreading the two halves of the hoof (also called toes or claws). This increases the likelihood of grabbing something rough or hold on a crack. *b)* when walking downhill, the higher compliance of the hoof in the lateral direction leads to a larger slip dissipation orthogonal to the direction of walking, providing a natural stabilizing effect. *c)* goats have a rough flexible traction pad in the lower part of the hoof; it is a shock absorber that also generates a friction force due to its texture and its capability of impressing in any irregularity of the terrain *d)* an additional brake force is generated by the soil or rocks stuck between the claws[10]. Consequently, our minimalistic design embodies most of these benefits and exploits passive dynamics to ensure an improvement on the stability with a low energy cost and without increasing the control complexity.

In this research, we attribute the passive stabilizing effect of the hoof to its morphological computation in dynamic contact with the ground that changes the work required to slip along a fixed distance and the behavior of the position, forces f_y and f_z, the angles of the joints θ and γ, and the vertical distance β during the transient state.

Using this novel passive dynamic foot, we demonstrate that the work required to slide the hoof over 2 different substrates (soft and rough bricks) is more than 3 times that needed for a rounded foot, the common approach for robotic feet. Besides, results show that during the transient each joint

The work described in this paper is supported in part by the Ecuadorian Government through SENESCYT, the U.K. Engineering and Physical Sciences Research Council (EPSRC) under Grants: EP/I028765/1, EP/I028773/1, EP/N03211X/1, and European Union H2020 project FourByThree code 637095.

[1]Sara-Adela Abad, Nantachai Sornkarn, Thrishantha Nanayakkara are with the Faculty of Natural and Mathematical Sciences, King/s College London, London, WC2R 2LS, UK (e-mail: sara.abad_guaman, nantachai.sornkarn, thrish.antha@kcl.ac.uk)

has a different effect over the displacements and forces.

The rest of the paper is organized as follows: Section II describes the biology of the goats' hoof and the design of our approach. Section III presents the experimental setup used to collect the data for the soft and rough terrain. Section IV explains and discusses the experiments and results obtained. Then, Section V presents the conclusions and future work.

II. Biologically Inspired Foot

In nature there is a myriad of hoofed animals. They share similar features such as hoofs, pads, and bone structure that suits their ecological niches. For instance, camels avoid sinking their feet in sand by using their 2 toes whose contact area with the ground increases due to their broad foot pad that flattens with the weight and the absence of the proximal interdigital ligament [11] which facilitate spreading their wide toes. However, they are prone to injuries in rocky terrain. On the other hand, pigs that are commonly found in soft terrains have 4 totally developed claws: 2 straight claws and 2 declaws (similar to those illustrated in Figure 1(b) as III and IV, and II and V, respectively). Declaws provide stability to the pig when the foot is sunk in the mud; therefore, they are smaller and higher than claws[12]. Nevertheless, among the ungulates, goats are well known for climbing trees and dams. The structure, size, and morphological computation of their hooves facilitates walking in terrain with high variability. Consequently, in this paper we analyze the morphological features of the hoof that increase the work required to slide the feet over two terrains.

A. Biological description of the hoof

Figure 1(b) illustrates the structure of the biological foot. The 2 halves of the hoof are called toes or claws. These toes are covered with hard keratin whose front side ends in a tip which allows digging into the soil for walking uphill. Additionally, mountain goats have a rough textured pad that is slightly projected over the nail to increase the friction with smooth surfaces and absorb shocks. The distal and proximal interdigital ligaments facilitate their locomotion in uneven terrain because they increase the likelihood of a toe to stand over firm terrain; furthermore, when walking downhill the higher compliance of the hoof in the lateral direction leads to a larger slip dissipation orthogonal to the direction of walking, which provides a natural stabilizing effect. Moreover, the rocks or soil stuck in the inter-digital cleft provides an extra brake [10]. To join the phalanges with the metacarpals and to provide mobility of the claws in the different planes, there are three joints: fetlock (metacarpophalageal), pastern (proximal interphalangeal) and the coffin (distal interphalangeal) joint. The mobility of the bones is controlled by flexor and extensor tendons.

B. Modeling

This research aims to understand the passive dynamics of the hoof. Therefore, as Figure 1 shows our design includes the fetlock, pastern, and coffin joints; the phalanges; the distal interdigital ligament; and tendons (substituted by antagonistic springs). To have a criterion to

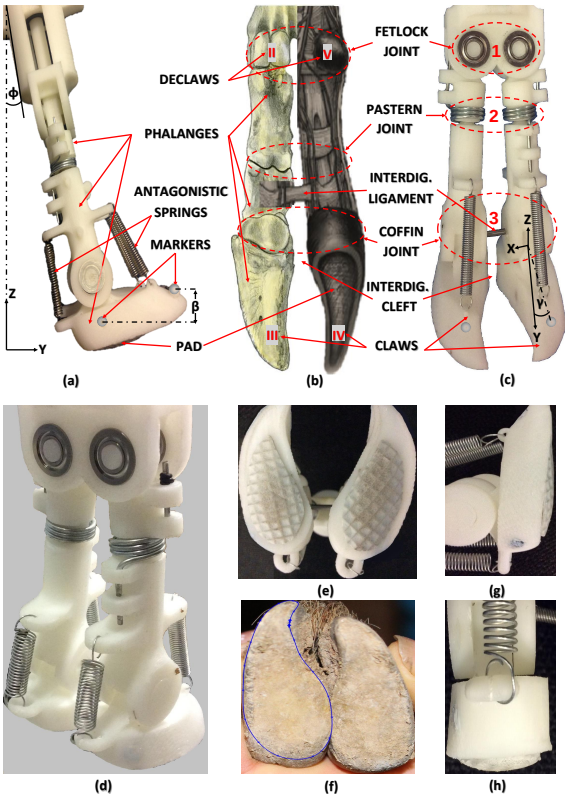


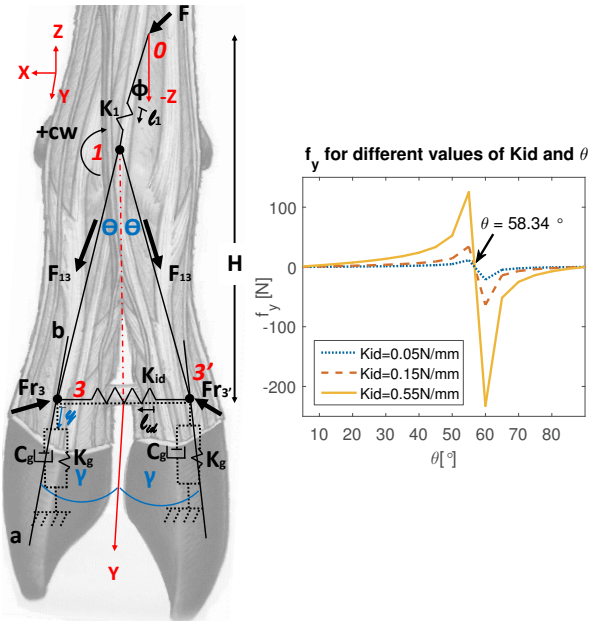
Fig. 1. Constructed and biological goats' hoof. a) Lateral view of the designed hoof in the setup. It shows the antagonistic springs that play the role of tendons in each claw. They passively control the tension and extension movements of the claw without adding an extra-weight and energy consumption. Additionally, the angle Φ and the distance β used in the mathematical model are also illustrated. b) Bones, ligaments, and external view of the biological foot (Courtesy: G. Constantinescu [13]). c) Frontal view and d) General view of the designed hoof. 2 pairs of bearings were used for the fetlock joints, 2 sets of 3 bearings for the pastern joints, and 2 bearings for the coffin joints. To set up the default position of the claws to the front, a torsional spring was placed on the pastern joint. For emulating the inter-digital ligaments, an extension spring was placed between the claws. Moreover, the angle γ is also introduced. e) Bottom view of the hoof: the rough shock absorber textured pad was emulated using a sole made of Ethylene-vinyl Acetate. f) Presents the profile of the hooves of an Ecuadorian mountain goat that was used for our design. g) The Lateral and h) Back view of the claw provide a better illustration of the slight projection of the pad over the nail.

analyze the morphological computation of the foot while it is in contact with the ground, the static model of the hoof, showed in Figures 1 and 2(a), was derived. The parameters and variables are described in Tables I and II. The forces of the system are: $\boldsymbol{F} = [0, f_y, -f_z]^T$; $\boldsymbol{N}_3 = [0, 0, K_g l_g]^T$, $\boldsymbol{F}_{r_3} = \left[-f_{r_x}, -f_{r_y}, 0\right]^T$, and $\boldsymbol{F}_{3/1} = -\boldsymbol{F}_{1/3} = f_{13}\left[-\sin\theta, -\cos\theta\sin\phi, \cos\theta\cos\phi\right]^T$. We assume a symmetric system; consequently, we only analyze for the contact point 3 and $l_{id} = L_{13}\sin\theta - 0.5L_{id}$. Firstly, we balance the forces in the system to obtain:

$$f_{r_y} = 0.5 f_y \tag{1}$$

$$f_z = -2K_g l_g \tag{2}$$

After, applying equilibrium conditions at segment 01 we find that $\boldsymbol{F} = \boldsymbol{F}_{K_1/1}$. Then, by balancing the forces at nodes we



(a) (b)

Fig. 2. a) Diagram of the Mathematical model of the hoof. b) Evolution of fy for different stiffness of the interdigital spring and θ values. It illustrates a critic point at θ_c=58.34[°]. Before this point f_y in the direction of the movement increases with K_{id} and θ to keep the equilibrium. Conversely, after θ_c, the system becomes unstable. Therefore, a force contrary to the direction of the movement has to be applied because claws tend to easily move apart from each other.

have:

$$f_y = 2f_{13}\cos\theta\sin\phi \rightarrow f_{13} = \frac{f_y}{2\cos\theta\sin\phi} \tag{3}$$

$$f_z = 2f_{13}\cos\theta\cos\phi \tag{4}$$

$$-K_g l_g = f_{13}\cos\theta\cos\phi \tag{5}$$

$$f_{r_x} + K_{id} l_{id} = f_{13}\sin\theta \tag{6}$$

Substituting f_{13} from equation (3) in equations (4), (5) and (6) we obtain:

$$f_z = f_y \cot\phi \tag{7}$$

$$-K_g l_g = 0.5 f_y \cot\theta \tag{8}$$

$$f_{r_x} = \frac{f_y \tan\theta}{2\sin\phi} - K_{id}(L_{13}\sin\theta - 0.5L_{id}) \tag{9}$$

Using (1), (8), and (9) in the relation $f_{r_x}^2 + f_{r_y}^2 = (\mu K_g l_g)^2$ we found:

$$f_y = \frac{2K_{id}(L_{13}\sin\theta - 0.5L_{id})}{\frac{\tan\theta}{\sin\phi} - \left(\mu^2\cot^2\phi - 1\right)^{1/2}} \tag{10}$$

This establishes a proportional relation between K_{id} and f_y that was evaluated using the values presented in Table II. As Figure 2(b) shows, there is a critical point at $\theta = 58.34$. Before this point the force required for the equilibrium of the system increases with K_{id} and θ. After this point the system becomes unstable. Therefore, a force contrary to the direction of the movement has to be applied because claws tend to easily move apart from each other.

TABLE I

ANALYZED VARIABLES

Description	Symbol	Units
Displacement of the foot along Y axis	y	mm
Force in the Y axis at point 0[1⋆]	f_y	N
Force in the Z axis at point 0[1⋆]	f_z	N
Position between the front and back of the claw[2⋆]	β	mm
Half the angle between the claws	θ	°
Angle between the right toe and the Y axis	γ	°

[1⋆] 0 is the point of connection between the XY table and the feet.
[2⋆] The distance was calculated along the Z axis.

TABLE II

VARIABLES AND PARAMETERS OF THE MODEL AND SIMULATION

Variables / Parameters	Symbol	Value	Units
Displacement of the spring K_1	l_1	-	mm
Displacement of the spring K_{id}	l_{id}	-	mm
Displacement of ground	l_g	-	mm
Natural length of spring K_{id}	L_{id}	-	mm
Mag. of the forces $\boldsymbol{F}_{K_3/1}$ and $\boldsymbol{F}_{K_{3'}/1}$	f_{13}	-	N
Normal Force at 3	$\boldsymbol{N}_3$	-	N
External force at 0 [1⋆]	$\boldsymbol{F}$	-	N
Friction Force between ground and claw	$\boldsymbol{F}_{r_3}$	-	N
Force of the spring K_1 over point 0	$\boldsymbol{F}_{K_1/0}$	-	N
Force of the spring K_1 over joint 1	$\boldsymbol{F}_{K_1/1}$	-	N
Force of the spring K_{id}	$\boldsymbol{F}_{K_{id}}$	-	N
Force from joint 3 to joint 1	$\boldsymbol{F}_{K_3/1}$	-	N
Force from joint 3' to joint 1	$\boldsymbol{F}_{K_{3'}/1}$	-	N
Static coefficient of friction	μ	1.7	
Angle between the foot and axis Z	ϕ	15	°
Stiffness of the interdigital spring[2⋆]	K_{id}	0.15	N/mm
Stiffness of the prismatic joint	K_1	363.63	N/mm
Stiffness of the ground	K_g	300	N/mm
Length of the link 13	L_{13}	110	mm

[1⋆] 0 is the point of connection between the XY table and the foot.
[2⋆] K_{id} has 3 values: $K_{id} = 0.05$[N/mm], $K_{id} = 0.15$[N/mm], and $K_{id} = 0.55$[N/mm]

C. Mechanical Design

As stated in Section I, the main limitation of robots for variable terrains are control complexity, power consumption, and stability. Therefore, a major challenge is to design a foot that passively adapts to the environment without affecting these parameters. To achieve our goal, the design is entirely comprised of passive elements and it was based on the hoof of an Ecuadorian mountain goat shown in Figure 1(f).

The hoof structure was constructed using a 3D printer with ABSplus as model material. Its total weight is 82.6g. Its height, illustrated in Figure 3(b), is 110mm, and the length of the claw is 55mm. The joints presented in Figure 1 were built using two stainless steel bearings of 6x12x3mm for the fetlock (metacarpophalangeal) joint, 3 stainless steels Metric Plain Bearing of 4x7x2.5mm for the pastern joints (proximal interphalangeal), and one 3D printed bearing for the coffin (distal interphalangeal) joint. To set up the default position of frontal end of the claws, torsional springs (PART NUMBER: LTMR100T 04 M and LTML100T 04 M for the left and right claws, respectively) were placed on the pastern joints. Figures 1(a) and (d) illustrate the antagonistic springs of the front and back (with stiffness $K_f = 0.15$N/mm and $K_b = 0.18$N/mm, respectively) of each claw that passively control its tension and extension movements. The interdigital ligament was replicated by an extension spring. At

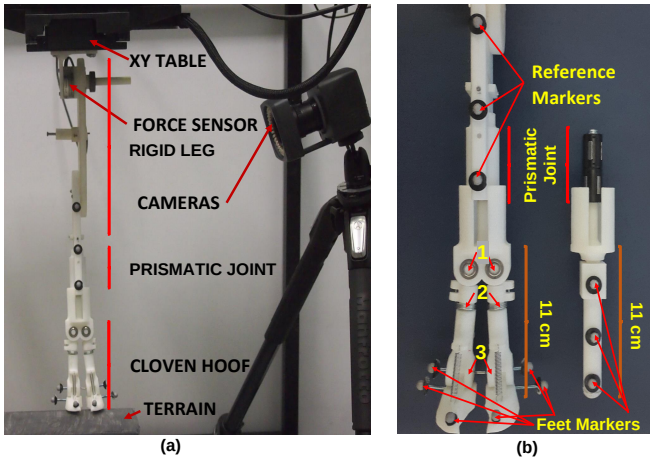


Fig. 3. Experiment setup. a) The foot is attached through the prismatic joint to the rigid leg while the force sensor couples this leg to the XY table that moves with a constant speed in the Y direction. 4 cameras were used to track the position of the markers of the claws. The tested surface were a red house brick and a wood brick covered with black plain paper. b) 11cm height feet utilized in the experiment. *Left:* Constructed hoof: It has 3 joints whose stiffness can be changed. *Right:* Rounded foot: it not only has the same length as the hoofed foot but also its contact area with the ground was covered with the same material of the pads of the claw.

the end, Figures 1(e),(g), and (h) exhibit the pad made of Ethylene-vinyl Acetate that is commonly used in slippers and sandals due to its low weight and moldability.

III. Experimental Setup

As figure 3 shows the foot is attached through a prismatic joint to the rigid leg. This joint contains the compression spring $K_1 = 363.63$N/mm for passively changing the normal force. The force sensor couples the rigid leg to the AEROTECH XY table type ANT130-160-XY-25DU-XY-CMS that moves with a constant speed of 10mm/s along the tested area. Moreover, for synchronizing the position and the force data, a delay of 5s at the beginning and end of each trial was set.

To identify the effect of passive dynamics on the transient state of the variables in Table I and work needed to slide the feet, the shape and joints' stiffness of the feet, presented in Figures 1(c) and 3(b), were changed according the 9 configurations summarized in Table III. Most of the joints were locked with clamps. Only, the antagonistic springs of joint 3 were fasten with metallic screws whose distances were those of the springs when the claw is perpendicular to the phalanges. Moreover, the interdigital spring K_{id} was utilized to stabilize joint 1 when it is set free. Finally, to passively join the back ends of the claws in the last configuration, a piece of fabric with a length of 5mm was employed. The force was measured at the top of the rigid leg using the MINI40 SI-40-2 sensor with a sampling frequency of 900Hz. This information was gathered using LabView2010 from National Instruments. Position data was collected at 150samples/s using VICON motion capture system. It has 4 VICON Bonita B10 cameras (250fps, 1megapixels) where 2 cameras were located at the front and 1 at each side of the foot. For tracking objects,

TABLE III

Experimental Feet Configurations

Name	Feet type	Free joints' name	K_{id}	Back ends state
ROUNDED	Rounded	-	-	free
HL	Hoof	-	-	free
H2	Hoof	2	-	free
H3	Hoof	3	-	free
H12_15	Hoof	1,2	0.15 N/mm	free
H123_5	Hoof	1,2,3	0.05 N/mm	free
H123_15	Hoof	1,2,3	0.15 N/mm	free
H123_55	Hoof	1,2,3	0.55 N/mm	free
H123_15B	Hoof	1,2,3	0.15 N/mm	linked

$Note$: In general, the notation $Hijk_stiffness$ denotes a hoof with joints $i,\ j,\ k$ free to move at a given stiffness. HL denotes a hoof with all joints locked. The configuration $H123_15B$ denotes a hoof with joints $1,\ 2$ and 3 free to move at stiffness $0.15N/mm$, and with the back-end of the hoof connected to represent the effect of the skin as shown in Figure 5.

3 markers with radius of 6.4mm were attached to each of them. The objects were the claws, the rounded foot, and the reference in the rigid leg.

MATLAB R2015b from MathWorks was employed for the VICON data acquisition process and experimental data analysis. For the statistical analysis of the work, its Statistics and Machine Learning Toolbox was utilized. Since the raw force data contained noise, it was filtered using the Wavelet toolbox (The Math Works Inc). Previous studies [14], [15] used the Mexican hat and Daubechies family (Db6), respectively, to analyze the frictional force. Nevertheless, in this paper the discrete wavelet transform was employed. Therefore, the Mexican hat was not taken into account because it is neither orthogonal nor biorthogonal. Criteria for selecting Haar wavelet with a decomposition level of 3 as a filter were as follows: the wavelet family was chosen based on the energy percentage that represents the data for all the samples where the low boundary for this energy was set to 97%; and, the decomposition level was selected depending on the highest energy corresponding to the details of the data using the previously selected wavelet.

In this research, we used 2 surfaces to analyze the effects of the type of feet, joint stiffness, and terrain on the transient state and the work(stability) required to slide the feet for the configurations summarized in Table III. The first tested surface was the smooth terrain (A). It was a wood brick covered with plain black paper whose length, width, and height were 20cm, 8.5cm, and 9cm, respectively. The second surface, named terrain (B), was a surface with a relatively high coefficient of friction. It was a red house brick whose length, width, and height were 19.8cm, 10cm, and 5cm, respectively. The probed distance was the width of the bricks which was aligned with the Y axis.

IV. Experiments and Results

Our main aims were to define the effect of morphological computation on: *A)* the work required to slip the hoof and the evolution during the transient state of *B)* the displacement, forces, relative position of the tip and back end of the toes, and *C)* angles θ and γ to interpret their effect on the stability.

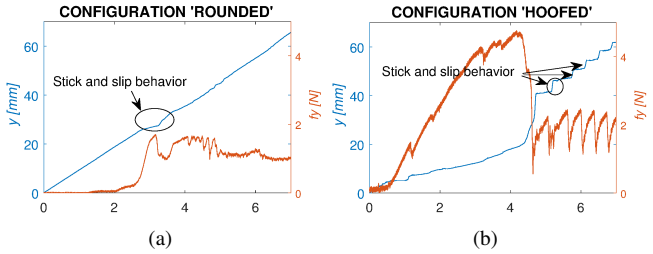


Fig. 4. Position and force in the Y axis measured over the smooth terrain for the configuration: a) ROUNDED: position presents a minimum stick slip behavior when the foot is moved along the width of the tested distance and its maximum force is lower than that of hoof. b) H123_55: the stick and slip behavior is notoriously bigger than the previous described configuration; as a result, it has a higher maximum force value. So, we can state that more work is going to be required to move hoofed configurations.

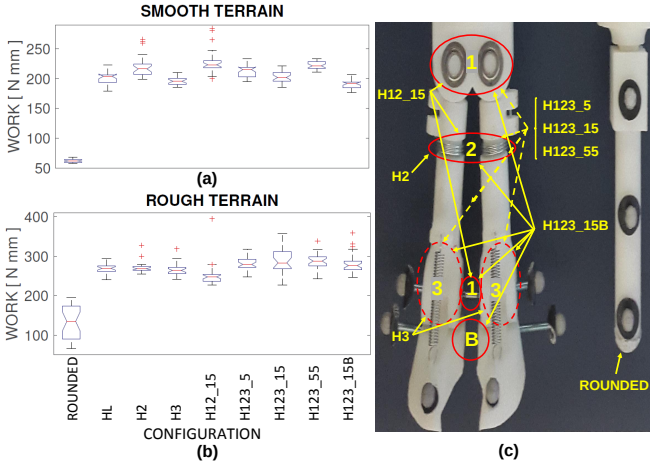


Fig. 5. Work required to slip the feet over the terrains. Anova test revealed that work depends not only on the terrain and foot configuration but also on the interaction feet-terrain. Therefore, over a) terrain A the work for moving the hoof was more than 3 times higher than that needed for the ROUNDED; additionally, the means of the configuration are different ($p<0.05$) which allows the analysis of the effect of the joints over the work. Similarly, in b) terrain B, with a higher coefficient of friction than the smooth terrain, the work for the hoofed configuration was more than twice that of the ROUNDED foot. Nevertheless, there was not enough evidence to state that the means of the configuration were different. As a result, only the data of terrain A was used for the analysis in the transient state.

As a consequence, we conducted 1 experiment for each type of terrain with 2 feet whose shape and joints stiffness were modified according the 9 configurations in Table III.

A. *Analysis of the work required to slip*

In this experiment, we explore the impact of the morphological computation over the work needed to slip the feet by changing the environment (terrains A and B) and stiffness of the joints (locked or unlocked). Additionally, we compare the performance of the hoof against the ROUNDED foot which is the common shape of the robots' feet.

Here the force and position for 30 trials for the 9 configurations for each type of terrain were collected. Figure 4 illustrates the raw data of the ROUNDED and H123_55 configurations for the smooth terrain. As can be seen, there is an stick and slip behavior that is more noticeable on the designed hoof than in the rounded foot because of the adaptability to the environment of the former. This increases the work required to slide the hoof. This work is presented in Figure 5 and calculated using Equation (11).

$$W = \int_a^b f(x)\delta(x), \tag{11}$$

where W is the work in Nmm, f is the force in Newtons, and x is the position in millimeters.

The advantage of using the hoof instead of the common approach (ROUNDED configuration) is more visible when we compare the average work required to slip the feet. Figure 5(a) illustrates that the average work required to slide the rounded foot in terrain A was 61.6595Nmm, whereas hoofed configurations required from 3.11 to 3.62 times higher that value. Similarly, Figure 5(b) reveals that for terrain B the work of the rounded foot was on average 134.8342Nmm, while the hoof needed from 1.84 to 2.13 times that value.

For understanding the effect of the environment over the work, we used statistical analysis. Firstly, the data was normalized; however, the One-sample Kolmogorov-Smirnov test revealed that it was not normally distributed. Therefore, it was transformed using the logarithm. The Anova (anova n) applied to the data of all the configurations of both terrains indicated that the work depends not only on the type of terrain and configuration but also on the interaction foot-terrain ($p<0.05$). Furthermore, the values of the same configuration but different terrain are statistically different ($p<0.05$).

To investigate the contribution of each joint, the data from each configuration within the same terrain was compared. However, for terrain B the work was mainly affected by the friction; therefore, there was not enough evidence to prove that the means were statistically different for some configurations. As a consequence, the subsequent analysis of this section are based only in the smooth terrain where the contribution of each joint was statistically differentiable. Moreover, to discriminate the effect of the stiffness of the joints and the friction between the hoof and the ground, our baseline configuration for comparing the increment of the work is *HL*. The results were obtained using the MannWhitney U test with a ($p<0.05$) at the 1% significance level. For analysis purposes, these results were divided depending on the number of locked joints and the stiffness of the interdigital spring in the following 3 groups:

Group 1) HL, H2, and H3: to discriminate the contribution of the joints, this group contains the configurations that have at most 1 free joint. Inside this group **H2** has the highest median; it is statistically different from the others ($p<0.05$); and its media is 9.7324% greater than that of *HL*. This suggest that friction between the pad and ground is not the only factor that opposes to the movement. In this case joint 2 presents an important role for avoiding slipping.

Group 2) H12_15, H123_15, and H123_15B: to differentiate the effect of the interaction between joints, these configurations have at least 2 free joints at the same time. The statistical analysis shows that all the means are different ($p<0.05$)

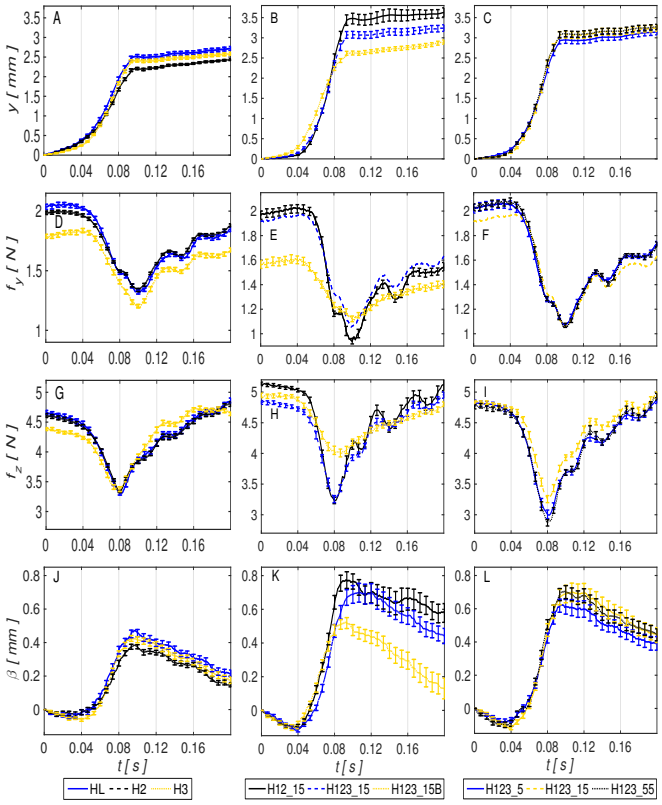


Fig. 6. Average and standard error of the data measured and calculated during the transient. Based on the work presented in Figure 5 the line colors yellow, blue, and black correspond to the lowest, medium, and highest work, respectively. The data is presented in 3 columns and 4 rows. The first column contains the configurations that have at most 1 free joint, second column at least 2 free joints, and in the last column the stiffness of the interdigital spring was changed. *Row1:* presents the position y (a, b, c), *Row2:* force f_y (d, e, f) along the Y axis; *Row3:* force f_z (g, h, i) along the Z axis; and *Row4:* the relative position β (j, k, l) of the tip with respect to the rear part of the toe.

and **H12_15** has the biggest median that is 13.0249% higher than that of *HL*. Nevertheless, as Figure 6(b) and Table IV reveal, the other configurations can have other features such as lower displacement and variability that also improve the stability.

Group 3) H123_5, H123_15, and H123_55: to comprehend the repercussion of the stiffness of the interdigital spring, it was changed to $K_{id} = 0.05N/mm$, $K_{id} = 0.15N/mm$, and $K_{id} = 0.55N/mm$. The analysis states that the medians are statistically different ($p<0.05$); and the highest work corresponds to **H123_55**. Its media is 10.6887% higher than the value of *HL*. However, as stated before the work depends on the type of terrain; consequently, for terrain B it exhibits a direct relation with K_{id}, whereas for the smooth terrain it has a different behavior. Nevertheless, in both terrains the maximum value correspond to the highest K_{id} value. To find the configuration with the highest work, H2, H12_15, and H123_55 were statistically compared, yet there was not enough evidence to state that they belong to different distributions. However, they have joint 2 in common that might be producing the highest slip dissipation.

TABLE IV

MEAN AND STANDARD DEVIATION OF Y[MM], f_y[N], AND f_z[N]

	y [mm]		f_y [N]		f_z [N]	
CONF.	**AVG**	**SD**	**AVG**	**SD**	**AVG**	**SD**
HL	1.758	0.315	1.734	0.124	4.273	0.356
H2	1.558	0.176	1.73	0.084	4.253	0.267
H3	1.652	0.209	1.585	0.135	4.254	0.261
H12_15	2.277	0.686	1.547	0.24	4.573	0.509
H123_5	1.998	0.441	1.622	0.174	4.246	0.39
H123_15	2.056	0.463	1.579	0.173	4.421	0.355
H123_55	2.084	0.42	1.628	0.149	4.241	0.389
H123_15B	1.874	0.318	1.377	0.206	4.542	0.34

B. Analysis of the position, forces, and relative positions during the transient for the hoofed configurations

This section analyzes the effect of the stiffness of each joint on the stability during the transient. However, data from terrain B and ROUNDED configuration was omitted because the analysis of the previous section showed that the distributions were not statistically different and the stick and slip behavior was almost at the minimum, respectively. Therefore, 60 samples that contain the slip and stick behavior from the 30 trials of the hoofed configurations in terrain A were extracted. Their average, AVG, and standard deviation, SD, values are summarized in Tables IV and V. Figure 6 compares their mean and standard errors in 3 groups or columns. Where *Group 1)* comprises *HL, H2, and H3*; *Group 2) H12_15, H123_15, and H123_15B*; and *Group 3) H123_5, H123_15, and H123_55*; and rows represent:

Row 1) Displacement y in the Y axis. This shows that joint 2 contributes to the stabilization because H2 has not only the lowest displacement between all the configurations but also Table IV states that it has the lowest variability among all the groups. Moreover, the comparison of the displacement of H2 within the first group, Figure 6(a), indicates that these variables depend not only on the number of free joints but also on which one was unlocked. Group 2, Figure 6(b), shows that the displacement increases with the degrees of freedom. In contrast, subfigure 6(c) shows that the displacement was minimally affected by the change of the stiffness of the K_{id} in Group 3. This result can be explained by the fact that the analysis in the previous subsection stated that the type of terrain has a significant influence; therefore in other environments K_{id} can play a more influential role. A similar behavior is observed in subfigures 6(f), (i), and (l).

Row 2) Figures 6(d),(e), and (f) illustrate how morphological computation affects f_y. Therefore, subfigure (d) shows that the mean value is affected by the stiffness where HL has the highest value and H2 and H3 had the lowest value. Additionally, subfigures (e)(f) state that joint 3 also affects the rate of change of this force. Consequently, those configurations that include this joint present smoother profiles. This can be explained by the fact that some energy is stored in the antagonistic springs. Conversely, the same subfigures illustrate that the interaction of joints 2 and 1 increases the rate of change of f_y. This is also supported by Table IV that presents a high variability of this interaction that contrast

TABLE V

AVERAGE AND STANDARD DEVIATION OF θ, γ, AND THE POSITION OF THE FRONTAL END OF THE CLAW WITH RESPECT TO ITS BACK END (β).

	θ [◦]		γ [◦]		$\beta[mm]$	
CONF.	**AVG**	**SD**	**AVG**	**SD**	**AVG**	**SD**
HL	4.586	0.0173	65.48	0.162	0.224	0.144
H2	4.58	0.0224	62.328	0.172	0.179	0.102
H3	10.11	0.0172	57.756	0.099	0.573	0.197
H12_15	9.894	0.1807	60.879	0.319	0.199	0.114
H123_5	10.98	0.6793	61.023	0.333	0.423	0.316
H123_15	9.731	0.2204	61.636	0.308	0.317	0.275
H123_55	9.463	0.0347	61.874	0.279	0.355	0.226
H123_15B	6.744	0.0678	52.332	0.193	0.229	0.265

with the low value of H2.

Row 3) On the other hand, subfigures 6(g), (h), and (i) support the relation between f_z and f_y presented in Equation 7 because when the feet are in contact with the ground, before 0.066s and after the force generated by the interaction body environment stops its motion at 0.1, both variables have similar profiles.

Row 4) subfigures 6(j), (k), and (l) suggest that there is a link between y and β because when comparing the last and first row of Figure 6, the configuration with the highest values in displacement also has those of β.Additionally, the profiles of β state that the hoof tends to stands over the tips to avoid slipping.

C. Analysis of the angles during the transient for the hoofed configurations

As Table V presents, the value of the angles θ, controlled by joint 1, and γ, controlled by joint 2, has a relatively low variability. Therefore, we chose only the configuration H123_55 to analyze the evolution of these variables. Figure 7 illustrates that the claw leaves the ground completely at 0.066s. As a result, θ increases the distance between the claws before this point to produce a larger slip dissipation orthogonal to the direction of walking. Thus, γ exhibits a decreasing behavior before 0.066s which resembles the human behavior of turning the feet inward for avoiding slipping in an inclined surface. Consequently, γ will increase while the claws are in the air because it tries to reach is default position. After the feet reached the ground and stick at 0.1s, both angles will change depending on the roughness of the terrain to improve the contact area between the foot and ground. Moreover, the hoof was stable during the experiments because θ never reached the critical value illustrated in Figure2(b). This can be a result of the lack of big irregularities on the terrains.

V. CONCLUSION

This paper for the first time shows how the the morphological computation contributes to increase the work required to slide a foot along certain distance and affects the displacement, forces, relative position, and angles during the transient without affecting the power consumption and control complexity. The results of this study indicate that each joint plays a different role which depends not only of the number of unlocked joint but also on the environment. Therefore, these findings can be applied in robots for all terrain conditions to improve their stability without affecting other critical variables. In the future, the hoof should be tested in legged locomotion with punctuated collision forces in unstructured terrain conditions.

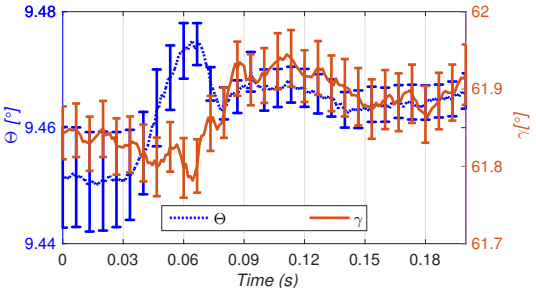


Fig. 7. Evolution of θ and γ during the transient for the H123_55 configuration. θ increases before sliding at 0.066s to increase the slip dissipation orthogonal to the movement direction. Conversely, γ decreases before 0.066s. While the hoof is in the air, both angles tend to recover their default position. Therefore, θ decreases while γ increases. Nevertheless, after reaching the ground both angles changed to improve the contact area between the foot and ground until t= 0.15s where γ tends to increases again.

REFERENCES

[1] N. Thrishantha, K. Byl, H. Liu, X. Song, and T. Villabona. "Dominant sources of variability in passive walking." In 2012 IEEE Int. Conf. on Robotics and Automation (ICRA), pp. 1003-1010. IEEE, 2012.

[2] M. Raibert, Legged robots that balance. Vol. 3. Cambridge, MA: MIT press, 1986.

[3] D. Wooden, M. Malchano, K. Blankespoor, A. Howardy, A. Rizzi, and M. Raibert. "Autonomous navigation for BigDog." In 2010 IEEE Int. Conf. on Robotics and Automation (ICRA), pp. 4736-4741. IEEE, 2010.

[4] M. Murphy, A. Saunders, C. Moreira, A. Rizzi, and M. Raibert, The littledog robot, Int. J. Rob. Res., pp. 1-5, 2010.

[5] A. S. Boxerbaum, J. Oro, G. Peterson, and R. D. Quinn, The latest generation Whegs^{TM}robot features a passive-compliant body joint, in Intelligent Robots and Systems, 2008. IROS 2008. IEEE/RSJ Int. Conf. on, 2008, pp. 1636-1641.

[6] U. Saranli, RHex: A Simple and Highly Mobile Hexapod Robot, Int. J. Rob. Res., vol. 20, pp. 616-631, 2001.

[7] M. M. Dalvand and M. M. Moghadam, Stair climber smart mobile robot (MSRox), Auton. Robots, vol. 20, pp. 3-14, 2006.

[8] J. B. Jeans and D. Hong, IMPASS: Intelligent Mobility Platform with Active Spoke System, 2009 IEEE Int. Conf. Robot. Autom., pp. 1605-1606, 2009.

[9] D. N. Beal, F. S. Hover, M. S. Triantafyllou, J. C. Liao, and G. V. Lauder, "Passive propulsion in vortex wakes", J. Fluid Mech., vol. 549, pp. 385-402, 2006.

[10] D. H. Chadwick, A beast the color of winter: the mountain goat observed, Bison Book. University of Nebraska Press, 2002.

[11] N. Jamal, Y. Mazaheri, and U. K. Mohabady, Gross anatomy of the ligaments of fetlock joint in dromedary camel, J. of Camel Practice and Research, 18.2, pp. 197-202, 2011.

[12] DYCE, K.M.; SACK, W.O.; WENSING, C.J.G., Miembros locomotores del cerdo, in Anatomia Veterinaria, 3th ed, Mexico: Elsevier, 2007, pp. 875-878.

[13] G. Constantinescu, Guide to Regional Ruminant Anatomy Based on The Dissection of The Goat, 1rst ed, Wiley, 2001, Fig. 2.10.

[14] Chen, C., Kovacevic, R., and Jandgric, D. Wavelet transform analysis of acoustic emission in monitoring friction stir welding of 6061 aluminum. Int. J. of Machine Tools and Manufacture, Vol. 43, no.13, pp. 1383-1390, 2003.

[15] Naerum, E., Cornella, J., and Elle, O. J. Wavelet networks for estimation of coupled friction in robotic manipulators. In Robotics and Automation, 2008. ICRA 2008. IEEE Int. Conf. on, pp. 862-867, May 2008.